Article

Assessing Dynamic Load Allowance of the Negative Bending Moment in Continuous Girder Bridges by Weighted Average Method

Yelu Wang [1,2], **Jun Tian** [3,*], **Yongjun Zhou** [1,*], **Yu Zhao** [1], **Wei Feng** [4] **and Keqiang Mao** [5]

1   School of Highway, Chang'an University, Xi'an 710064, China
2   Key Laboratory of Bridge Detection Reinforcement Technology Ministry of Communications, Xi'an 710064, China
3   Department of Civil Engineering, Ordos Institute of Technology, Ordos 017000, China
4   Xi'an Municipal Engineering Design & Research Institute Co., Ltd., Xi'an 710064, China
5   Shan Dong Hi-Speed Yanwei Expressway Co., Ltd., Yantai 264043, China
*   Correspondence: lele1008@oit.edu.cn (J.T.); zyj@chd.edu.cn (Y.Z.); Tel.: +86-47-7859-0272 (J.T.); +86-029-8233-4872 (Y.Z.)

Abstract: Accurate acquisition of dynamic load allowance (DLA) based on measurement data is essential to the safety assessment of a bridge. When static load tests cannot be achieved, and filtering fails, the estimated DLAs from the experimental method vary widely due to the choice of a left or right band. In this paper, the proposed weighted average method (WAM) is used to possibly solve the above problem in continuous gird bridges. Two-span and three-span precast concrete box-gird bridges were selected to optimize intercepted segments of WAM for the first time with the assistance of standard deviation and coefficient of variation in statistics. Then, a DLA measurement case of the negative bending moment was utilized to verify the validity of the WAM. The results show that the intercepted segments of 10/16 to 1 times the span length were suitable for the WAM to calculate the DLA of the negative bending moment due to small offset moments and stable variation coefficients. The WAM had a strong anti-interference ability of outliers filtering in "bad data," which differed significantly from the experimental method. In three measurements of a field bridge, DLAs obtained by the WAM had less dispersion than the experimental and low-pass filtering methods.

Keywords: bridge engineering; dynamic load allowance; weighted average method; vehicle-bridge coupled; negative bending moment

1. Introduction

The dynamic effect of moving vehicles on bridges is generally treated as a dynamic load allowance (or dynamic impact factor), which is one of the important evaluation indicators of bridge health. Failure to properly account for dynamic effect can underestimate the stress cycles contributing to bridge component fatigue [1,2].

Presently, some disagreement exists between provisions of various national bridge codes because dynamic load allowance (DLA) depends, in addition to the maximum span or the natural frequency, on many other parameters that were difficult to consider with reasonable accuracy [3–5]. These provisions can be divided into two categories: (1) continuous functions: for example, the DLA in MTPRC (2015) code is determined by the structure frequency [6], and the JRA code is related to the bridge span and structure type [7]. (2) Discrete functions: for example, CHBDC (2017) code is based on the type and number of axles, AASHTO (2017) code is related to limit state [8], and Austroads (2004) code is given based on traffic load models. However, the prerequisite of these codes for specifying DLA is to identify the accurate measurement value. Then, DLA's empirical formulas or values are further determined for design in combination with numerical analysis. Therefore, accurate

acquisition of DLAs based on measurement data is essential to the safety assessment of bridges.

Various definitions have also been used to quantify DLA, leading to different conclusions from the same data. Mclean and Marsh [1] mentioned three common definitions for DLA, where all methods use the ratio of dynamic response to static response as the basic principle. A major difference is the acquisition of static response. The static response can be calculated by analysis, while multiple static load tests or filtering in a field. Sometimes, finding the mean responses by automatic filtering is made difficult when the period of static oscillations matches the period of dynamic oscillations. It is also difficult to keep the vehicle in the same lane during the two tests (static and dynamic load tests). Therefore, a static response is typically replaced by the equivalent mean response from the dynamic response curve [9]. Nevertheless, in practice, different choices may lead to a significant difference in DLAs because there are two minimal values near the maximum dynamic.

Two other issues with DLA were mentioned in our previous study. One is DLA should be considered for all the impact of the design vehicles on all positions, and the other one is the time hysteresis of dynamic response [10,11]. As shown in Equation (1) and Figure 1, the static response of the bridge caused by the design vehicle is equivalently amplified by μ, and μ should synthetically represent the sum effect caused by each axel as much as possible. Usually, this μ is only calculated by the maximum dynamic response point, which is not necessarily the point of interest when checking for fatigue stresses. Therefore, we have proposed the weighted average method (WAM) to address the above issues [11]. In addition, unrealistic responses of the bridge have been monitored recently, as shown in [12]. Deflections were contaminated by two high-frequency peaks, which are important for calculating DLA. When static load tests cannot be achieved, and filtering fails, the WAM also seems to be an optimal method for dealing with the outliers described above.

$$S_d = (1 + \mu)\sum P_i y_i = (1 + \mu)S_t \tag{1}$$

where S_d is the maximum dynamic response of a bridge under the moving vehicles for the design purpose; μ is the bridge's integrated (or total or equivalent) DLA for the design purpose. P_i is the weight of the axle; S_t is the static design response of the bridge.
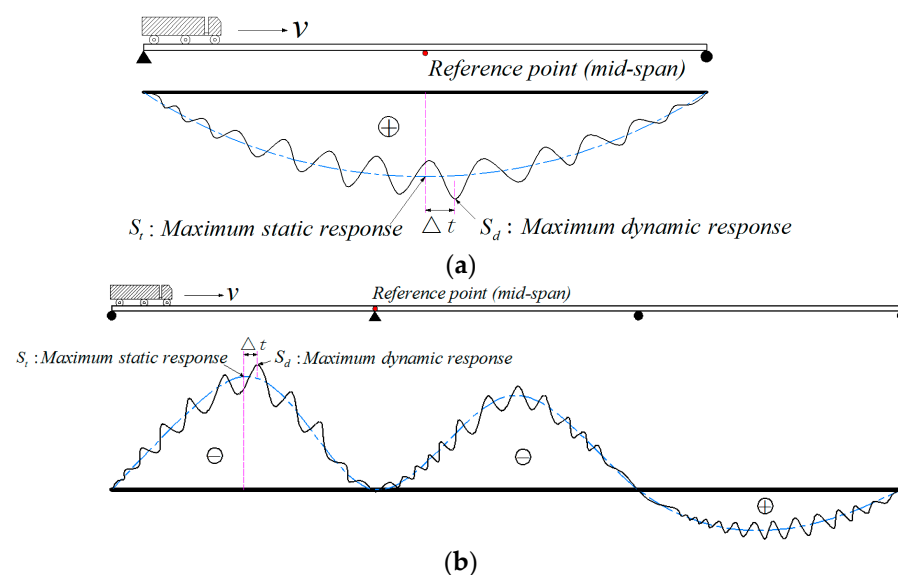

(a)

(b)

Figure 1. Time-history curves of static and dynamic response due to vehicles. (**a**) Response of a simply supported girder bridge; (**b**) Response of a continuous girder bridge. Δt is the hysteresis time between dynamic and static response. ⊕ represents the positive effect; ⊖ represents the negative effect conversely.

Moreover, available studies have revealed that road surface condition, bridge structure, traveling speed, and vehicle parameters (axle weight, wheelbase, and vehicle suspension) affect DLA [13–16]. Ma et al. [17] demonstrated that the dynamic response of the elastically supported bridge increases with decreasing bridge span and vehicle weight and the deterioration of road profile and support boundary. Gao noted that for continuous girder bridges, the frequency of the bridge decreases with the number of spans, and the DLA of the side spans is different from that of the other spans [18]. Deng et al. [19] concluded that the DLAs of continuous gird bridges increase greatly with road surface conditions. The effect of vehicle speed on DLA remains controversial, with some monotonically increasing and others with no obvious regularities [20,21]. Among all the parameters, road surface condition is still the most significant influencing factor [15].

Our previous research proposed the weighting method and successfully applied it in simply supported girder bridges. The use of whole measurement data to calculate DLA has been shown reasonable due to only one positive bending moment zone in these bridges. However, it has not been demonstrated in continuous girder bridges with multiple zones and negative moment effects, as shown in Figure 1b. This study is a continuation of our previous work. It differs from the previous study in that the WAM was first attempted for the calculated DLA of the negative bending moment in a continuous girder bridge. Meanwhile, standard deviation and coefficient of variation in statistics were adopted for the first time to optimize the weighted segments. This paper chose two-span and three-span precast concrete box-gird bridges as the subject of study. The time-history curves of the bridges for 25 conditions were obtained by orthogonal tests and vehicle-bridge interaction analysis (VBI). The discreteness and variability of the DLAs calculated by the WAM were assessed with the assistance of standard deviation and coefficient of variation. Optimal intercept segments were determined finally, and an engineering case verified the applicability of WAM in continuous girder bridges.

2. Existing DLA Methods

2.1. Theoretical Method

The dynamic amplification factor is the ratio of the bridge's maximum dynamic response (Y_{max}) to the maximum static response (Y_{st}) under the same vehicle load. The difference between the DLA (u) and the dynamic amplification factor (DAF) is 1, as shown in Equation (2). The diagram of this method is shown in Figure 2, and the related DLA is named theoretical DLA.

$$DAF = 1 + \mu_d = \frac{Y_{max}}{Y_{st}} \tag{2}$$

where DAF is the dynamic amplification factor; μ_d is the dynamic load allowance calculated by definition; Y_{max} and Y_{st} are the maximum dynamic response and its corresponding static response of a bridge under the same vehicle load in non-design conditions, respectively.
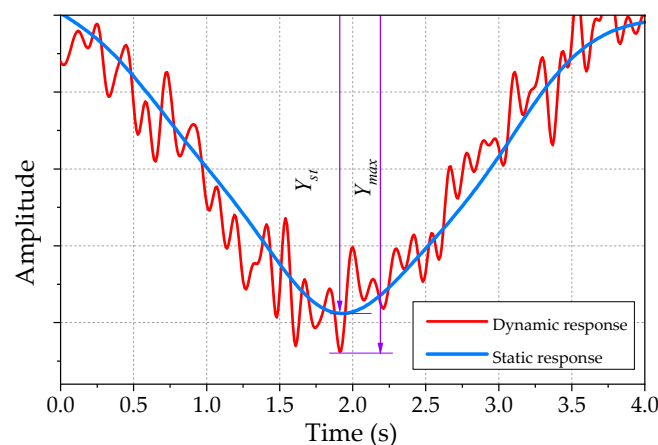

Figure 2. Principle of conventional DLA.

2.2. Experimental Method

Since it is difficult to get the static response, it is typically replaced by the equivalent mean response (Y_{mean}) from the dynamic response curve [9], as shown in Equation (3). DLA by this method is denoted as experimental DLA, and the details are shown in Figure 3.

$$\begin{cases} 1 + \mu_m = \frac{Y_{max}}{Y_{mean}} \\ Y_{mean} = \frac{1}{2}(Y_{max} + Y_{min}) \end{cases} \tag{3}$$

where μ_m is the DLA calculated by the experimental method; Y_{mean} is the equivalent mean response, which is approximately equal to the average of the Y_{max} and Y_{min}.
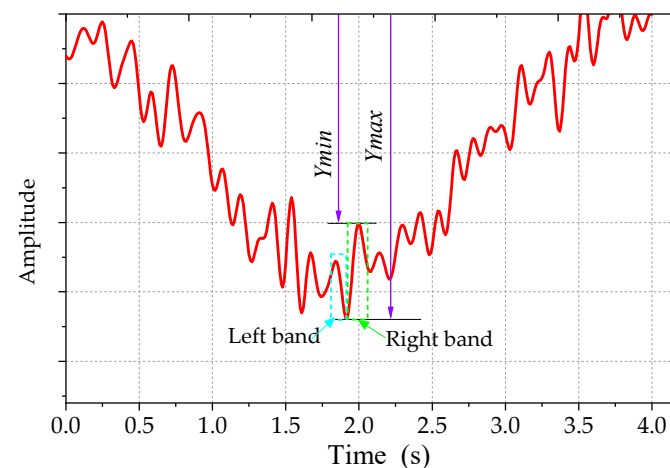

Figure 3. Principle of the DLA by experimental method.

This definition can give fairly reliable results because it was obtained from the calibration test that the maximum static load response is close in magnitude to the corresponding mean response. In the field test, the maximum dynamic response can be obtained from the time-history curve of the vehicle-bridge coupled vibration. In contrast, the maximum static response can be extracted using the Taylor series or filters [22]. Still, in filtering, it is essential to ensure that the filtered waveform cannot be time-shifted. The reasonable cut-off frequency is also critical. However, there is still no standard available for filtering; the low range passing filter of 0.6 to 2.0 Hz is recommended [23–25].

2.3. Proposed Weighted Average Method

The WAM, which we proposed, takes per wave crest corresponding to its wave trough as a local band, divides the obtained dynamic response (time-history curve) into a finite number of units, and then weights each unit according to its participation [11], as shown in Figure 4 and Equations (4)–(7). The DLA from the WAM was denoted weighted DLA. The calculation process is expressed as follows:

$$\overline{\mu} = \sum_{i=1}^{n} u_i v_i \qquad (i = 1, 2, 3, \ldots, n) \tag{4}$$

$$v_i = \frac{Y_{meani}}{\sum\limits_{i=1}^{n} Y_{meani}} \tag{5}$$

$$u_i = \frac{Y_{maxi}}{Y_{meani}} \tag{6}$$

$$Y_{meani} = \frac{(Y_{mini} + Y_{maxi})}{2} \tag{7}$$

where u_i is the DLA calculated by the ith local band; Y_{meani} is the ith local "static" response corresponding to u_i in the time-history curve; Y_{maxi} is the maximum response of the ith local band; n is the regular number of the local band appeared in the time-history course curve; v_i is the weight of the DLA of the ith local band.
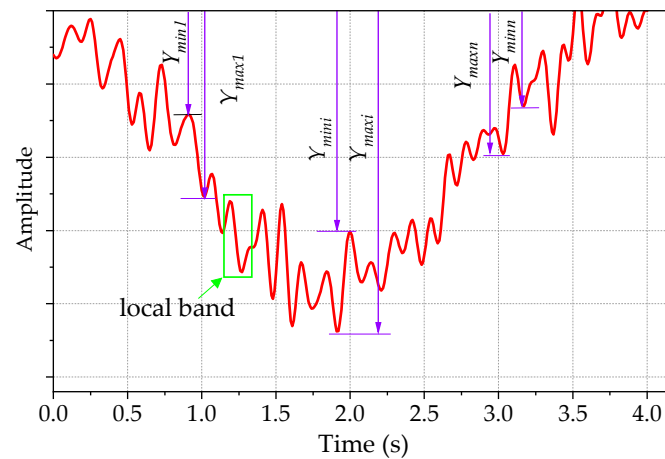

Figure 4. Principle of the WAM.

3. Bridge and Vehicle Analysis Models

3.1. Vibration Equation

Taking a three-axle vehicle as an example, ignoring the local vibrations inside the vehicle, the vehicle body was assumed to be rigidly coupled and supported on a suspension-spring system and wheels. Both the wheels and the suspension system were considered elastomers whose damping was proportional to speed. Ultimately, the vehicle was simplified to a spring-mass model with five independent DOFs, as shown in Figure 5. The corresponding parameters of the vehicle are shown in Table 1 [26,27]. The vibration equation for this vehicle model was expressed as follows:

$$M_v \ddot{Z}_v + C_v \dot{Z}_v + K_v Z_v = G_v + F_{bv} \tag{8}$$

$$[M_v] = \begin{bmatrix} m_1 & 0 & 0 & 0 & 0 \\ 0 & m_2 & 0 & 0 & 0 \\ 0 & 0 & m_3 & 0 & 0 \\ 0 & 0 & 0 & M\beta_3^2 + I_\alpha/l_u{}^2 & M\beta_3(\beta_1+\beta_2) - I_\alpha/l_u{}^2 \\ 0 & 0 & 0 & M\beta_3(\beta_1+\beta_2) - I_\alpha/l_u{}^2 & M(\beta_1+\beta_2)^2 + I_\alpha/l_u{}^2 \end{bmatrix}$$

$$[K_v] = \begin{bmatrix} k_{s1} + k_{t1} & 0 & 0 & -k_{s1} & 0 \\ 0 & k_{s2} + k_{t2} & 0 & -(\beta_2+\beta_3)k_{s2} & -\beta_1 k_{s2} \\ 0 & 0 & k_{s3} + k_{t3} & 0 & -k_{s3} \\ -k_{s1} & -(\beta_2+\beta_3)k_{s2} & 0 & k_{s1} + (\beta_2+\beta_3)^2 k_{s2} & \beta_1(\beta_2+\beta_3)k_{s2} \\ 0 & -\beta_1 k_{s2} & -k_{s3} & \beta_1(\beta_2+\beta_3)k_{s2} & \beta_1^2 k_{s2} + k_{s3} \end{bmatrix}$$

$$[C_v] = \begin{bmatrix} c_{s1} + c_{t1} & 0 & 0 & -c_{s1} & 0 \\ 0 & c_{s2} + c_{t2} & 0 & -(\beta_2+\beta_3)c_{s2} & -\beta_1 c_{s2} \\ 0 & 0 & c_{s3} + c_{t3} & 0 & -c_{s3} \\ -c_{s1} & -(\beta_2+\beta_3)c_{s2} & 0 & c_{s1} + (\beta_2+\beta_3)^2 c_{s2} & \beta_1(\beta_2+\beta_3)c_{s2} \\ 0 & -\beta_1 c_{s2} & -c_{s3} & \beta_1(\beta_2+\beta_3)c_{s2} & \beta_1^2 c_{s2} + c_{s3} \end{bmatrix}$$

$$\{G_v\} = \{m_1 g, m_2 g, m_3 g, Mg\beta_3, (\beta_1+\beta_2)Mg\}^T$$

$$\{F_{bv}\} = \{k_{t1}y_1 + c_{t1}\dot{y}, k_{t2}y_2 + c_{t2}\dot{y}_2, k_{t3}y_3 + c_{t3}\dot{y}_3, 0, 0\}^T$$

where M_v, C_v and K_v are the mass, damping, and stiffness matrices of the vehicle, respectively; F_{vb} is the vector of the vehicle-bridge interaction (contact) forces acting on the vehicle; G_v is gravity force vector; Z_v, $\dot{Z}_v$ and $\ddot{Z}_v$ are the displacement, velocity, and acceleration vectors of the vehicle, respectively.
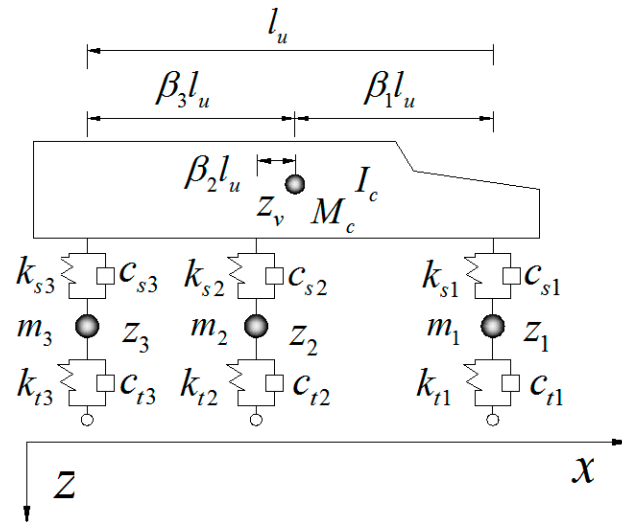

Figure 5. Vehicle model with three-axis.

Table 1. Parameters of the vehicle.

Parameter	Value
Pitching moment of inertia of truck body $I_c/(\text{kg·m}^2)$	55,502
Mass of the first, second, and third suspension $m_i/(\text{m/kg})$	500
Upper spring stiffness of the first axle $k_{s1}/(\text{N·m}^{-1})$	251,380
Upper spring stiffness of the second and third axle k_{t2}, $k_{t3}/(\text{N·m}^{-1})$	2,064,000
Upper damper coefficient of the first axle $c_{s1}/(\text{N·s·m}^{-1})$	50,636
Upper damper coefficient of the second and third axle k_{t2}, $k_{t3}/(\text{kN·s·m}^{-1})$	25,320
Lower spring stiffness of the first axle $k_{s1}/(\text{N·m}^{-1})$	1,100,000
Lower spring stiffness of the second and third axle k_{s2}, $k_{s3}/(\text{N·m}^{-1})$	2,200,000
Lower damper coefficient of the first axle $c_{s1}/(\text{N·s·m}^{-1})$	3500
Lower damper coefficient of the second and third axle k_{t2}, $k_{t3}/(\text{N·s·m}^{-1})$	7000
$l_u/(\text{m})$	5
$\beta_2 l_u/(\text{m})$	1.06
$\beta_3 l_u/(\text{m})$	1.3

The bridge vibration equation was expressed as follows:

$$M_b\ddot{Y}_b + C_b\dot{Y}_b + K_bY_b = F_{vb} \tag{9}$$

where M_b, C_b and K_b are the mass, damping, and stiffness matrices of the bridge, respectively; Y, $\dot{Y}$ and $\ddot{Y}$ are the displacement, velocity and acceleration vectors of the bridge, respectively; F_{vb} is the vector of the vehicle–bridge interaction (contact) forces acting on the bridge.

If the vehicle and the bridge were considered as two separate systems, the coupling between the two was linked by the interaction between the tire and the bridge deck, as shown in Figure 6. The interaction force between the tire and the bridge was described as:

$$F_{ti} = k_{ti}u_i + c_{ti}\dot{u}_i \tag{10}$$

where F_{ti} is the vehicle-bridge interaction (contact) forces acting on the bridge; k_{ti}, and c_{ti} are the stiffness and damping coefficient of the ith tire; u_i and $\dot{u}_i$ are the vertical displacement and velocity of the ith tire contact with the bridge.
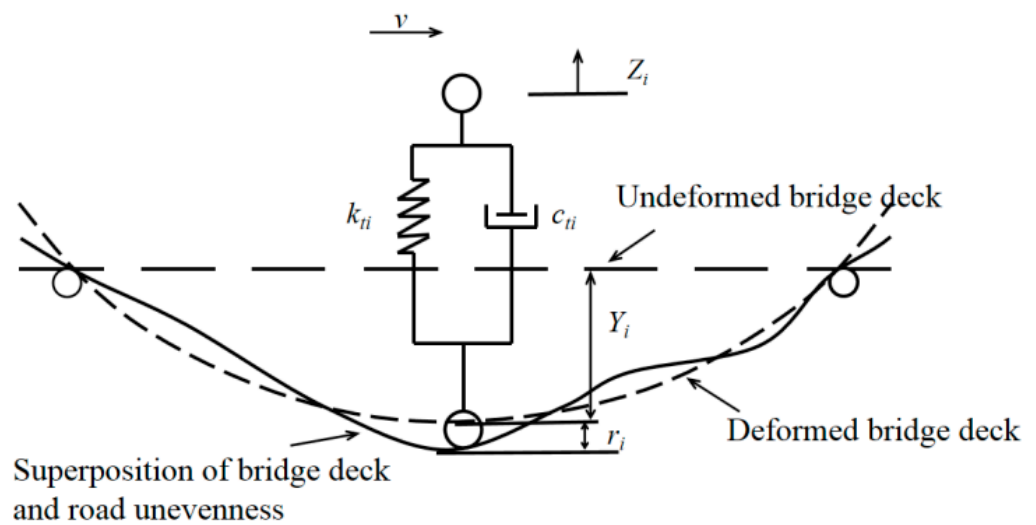
Figure 6. Mechanical model of wheel-bridge contact.

The vehicle-bridge coupling vibration equation system could be obtained by combining Equations (8)–(10) as follows:

$$\begin{bmatrix} M_b & \\ & M_v \end{bmatrix}\begin{Bmatrix} \ddot{Y}_b \\ \ddot{Z}_v \end{Bmatrix} + \begin{bmatrix} C_b & C_{bv} \\ C_{vb} & C_v \end{bmatrix}\begin{Bmatrix} \dot{Y}_b \\ \dot{Z}_v \end{Bmatrix} + \begin{bmatrix} K_b & K_{bv} \\ K_{vb} & K_v \end{bmatrix}\begin{Bmatrix} Y_b \\ Z_v \end{Bmatrix} = \begin{Bmatrix} G_v + F_{bv} \\ F_{vb} \end{Bmatrix} \tag{11}$$

where K_{bv}, K_{vb}, C_{vb}, and C_{bv} are the damping and stiffness coupling matrices of the vehicle-bridge, respectively.

The vehicle equation (Equation (8)) and the bridge equation (Equation (9)) are independent equations, while the vehicle-bridge coupled vibration equation system (Equation (11)) becomes non-independent due to the introduction of mutual interaction force (Equation (10)). The analytical solution cannot be obtained because Equation (11) is a higher-order inhomogeneous system of differential equations, which could be solved by numerical solution methods [28–32]. The Newmark-β in the direct integration methods (step-by-step integration) was used in this paper [5,33]. The vehicle and bridge were considered as two subsystems and modeled accordingly in the ANSYS workbench. The transmission of mutual interaction forces linked the two systems. Assuming that the displacement u_i, velocity $\dot{u}_i$ and acceleration $\ddot{u}_i$ of a bridge under the vehicle at time t_i were known, the displacement u_{i+1}, velocity $\dot{u}_{i+1}$ and acceleration $\ddot{u}_{i+1}$ of a bridge at the time t_{i+1} were obtained using Equations (12)–(14). According to the changing time and position of the vehicle acting on the bridge, the coupled vibration responses of the bridge and vehicle were solved sequentially based on the ANSYS solver. The specific solution procedure can be referenced in [34]. Figure 7 shows in detail the flow of this process.

$$(a_0[M] + a_1[C] + [K])\{u_{i+1}\} = \begin{aligned} &\{F_{i+1}\} + [M]\big(a_0\{u_i\} + a_2\{\dot{u}_i\} + a_3\{\ddot{u}_i\}\big) + \\ &[C]\big(a_1\{u_i\} + a_4\{\dot{u}_i\} + a_5\{\ddot{u}_i\}\big) \end{aligned} \tag{12}$$

where $a_0 = \frac{1}{\alpha\Delta t^2}$, $a_1 = \frac{\delta}{\alpha\Delta t}$, $a_2 = \frac{1}{\alpha\Delta t}$, $a_3 = \frac{1}{2\alpha} - 1$, $a_4 = \frac{\delta}{\alpha} - 1$, $a_5 = \frac{\Delta t}{2}\left(\frac{\delta}{\alpha} - 2\right)$, $\delta = 1/2$, $\alpha = 1/4$.

$$\{\ddot{u}_{i+1}\} = a_0(\{u_{i+1}\} - \{u_i\}) - a_2\{\dot{u}_i\} - a_3\{\ddot{u}_i\} \tag{13}$$

$$\{\dot{u}_{i+1}\} = a_1(\{u_{i+1}\} - \{u_i\}) - a_4\{\dot{u}_i\} - a_5\{\ddot{u}_i\} \tag{14}$$

```
                              Begin

  Enter the information of the        Enter the parameters of the bridge
      vehicle and lane

  Form the stiffness, mass and        Form the stiffness, mass and
  damping matrices of the vehicle     damping matrices of the bridge

          The initial displacement of the vehicle and bridge
                        at a given time t

          Calculate the position, number of the wheels, and
                  the number of vehicles on the bridge

          Determine the birdge roughness value at each
                wheel based on the  roughness sample

          Calculate the initial interaction force according to
           the  geometric equation of wheel- bridge contact

          Solve the vehicle vibration equation to obtain the
               vehicle displacement at the current moment

          Calculate the interaction force of vehicel and
                            bridge

          Solve the bridge vibration equation to obtain the
               Bridge displacement at the current moment

               Whether the bridge                No
               displacement converges

                             Yes

               Whether the vehicles              No
               are all out of the bridge

                             Yes

          Obtained the time-history curve

                              End
```
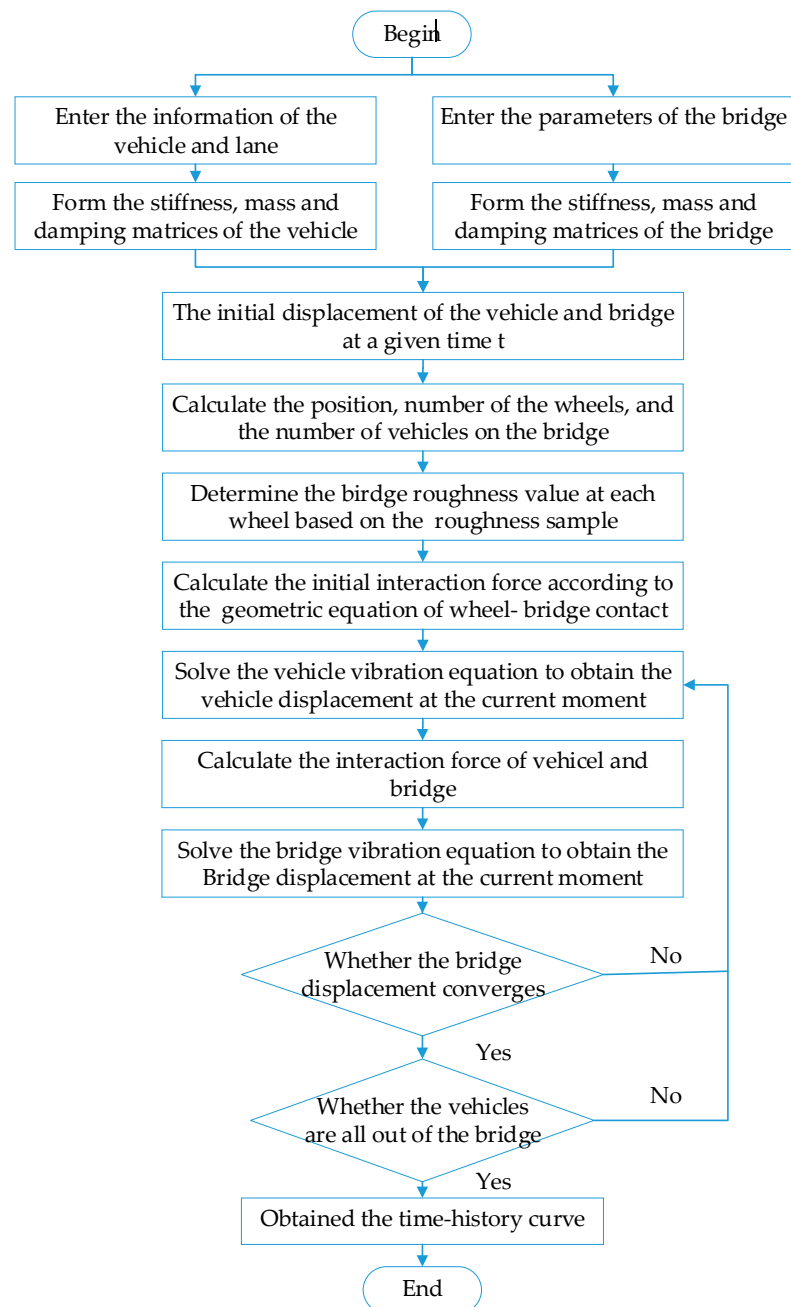
Figure 7. Solution flow of the vehicle-bridge coupled vibration.

3.2. Negative Moment Responses of the Continuous Box-Girder Bridge

Taking precast concrete continuous box-girder bridges as examples, the cross-section is shown in Figure 8; The FEM was established by ANSYS software. Beam188 elements simulated the girder, the damping ratio was 0.05, and the model is shown in Figure 9, with the following basic assumptions:

(1) The wheels always kept in contact with the bridge during moving, while only the vertical vibration of the vehicle was considered;
(2) The stiffness and damping of the bridge should be evenly distributed within the length of the bridge span;
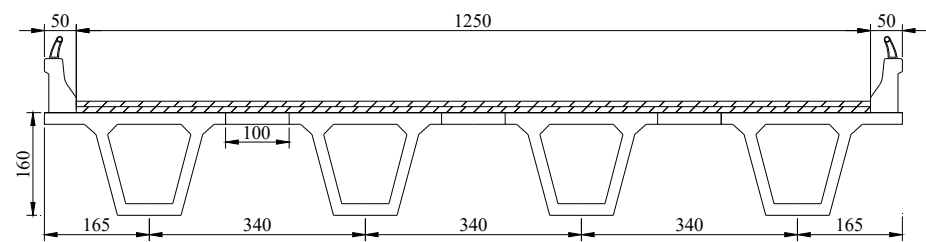(3) The deformations of the structure satisfied Hooke's law.

Figure 8. Cross-section of the precast concrete continuous box-gird bridge (unit: cm).
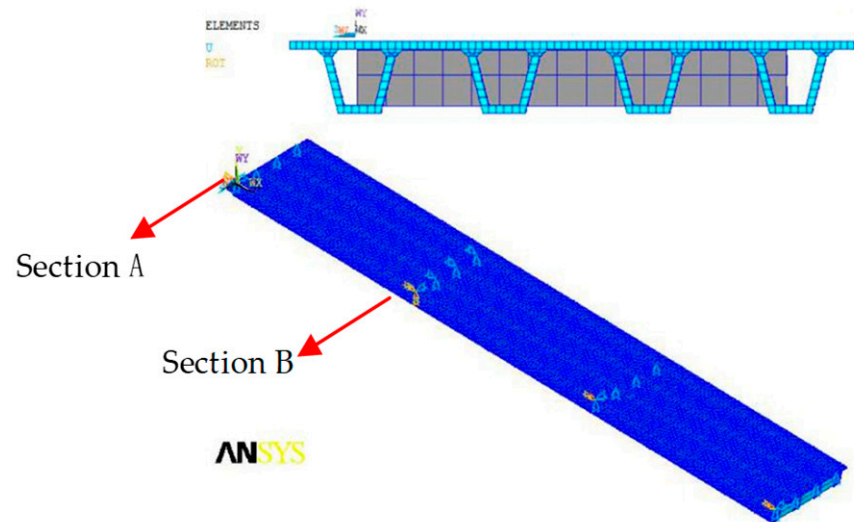

Figure 9. Model of the precast concrete box-gird bridge.

The sensitive parameters on the DLA of bridges were considered, such as bridge span length, driving speed, road surface condition, and vehicle weight, to solve the dynamic response of the negative bending moment of the continuous girder bridge. Considering many full-scale test conditions, an orthogonal test design was used to select representative conditions for the calculation (Figure 10). The condition parameters of the orthogonal test are shown in Table 2. The negative moment responses (or time-history curves) of typical conditions for two-span continuous gird bridges and three-span continuous gird bridges are shown in Figures 11 and 12.
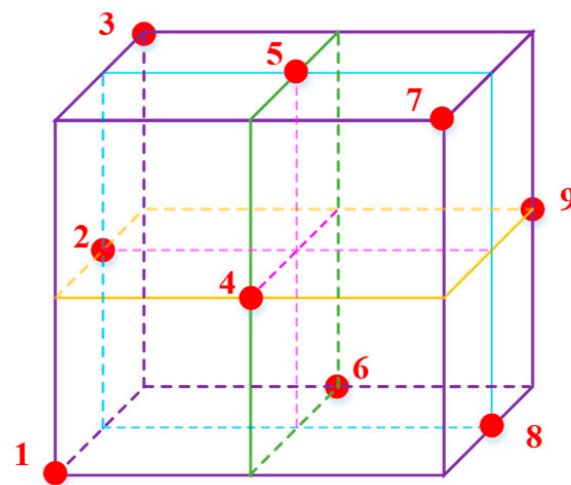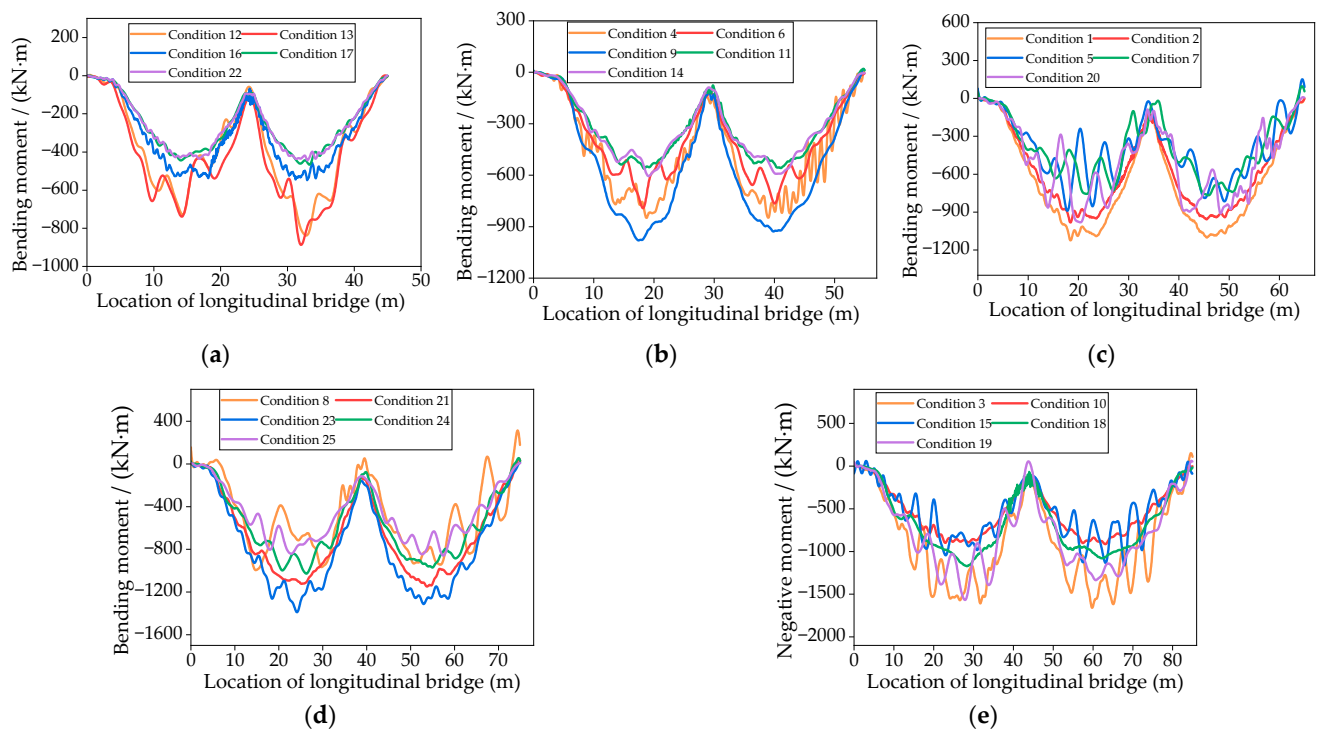

Figure 10. Schematic of orthogonal test design.

Figure 11. Time-history curves of the negative bending moment in the two-span continuous girder bridges. (**a**) Time-history curves of the bridges with a span of 20 m; (**b**) Time-history curves of the bridges with a span of 25 m; (**c**) Time-history curves of the bridges with a span of 30 m; (**d**) Time-history curves of the bridges with a span of 35 m; (**e**) Time-history curves of the bridges with a span of 40 m.

Table 2. Parameters of each condition.

Conditions	Span (m)	Velocity (km/h)	Road Surface Condition	Vehicle Weight (ton)
1	30	30	A	35
2	30	30	A	30
3	40	60	C	35
4	25	30	D	30
5	30	90	C	20
6	25	30	C	25
7	30	120	B	20
8	35	120	D	20
9	25	120	A	35
10	40	30	A	20
11	25	90	A	20
12	20	120	C	30
13	20	90	D	35
14	25	60	B	20
15	40	30	D	20
16	20	30	B	25
17	20	60	A	20
18	40	120	A	25
19	40	90	B	30
20	30	60	D	25
21	35	60	A	30
22	20	30	A	20
23	35	30	B	35
24	35	90	A	25
25	35	30	C	20

Denotes: Four different road surface conditions were used in the study: 'very good', 'good', 'average', 'poor'. Detailed parameters could be referred to [20].
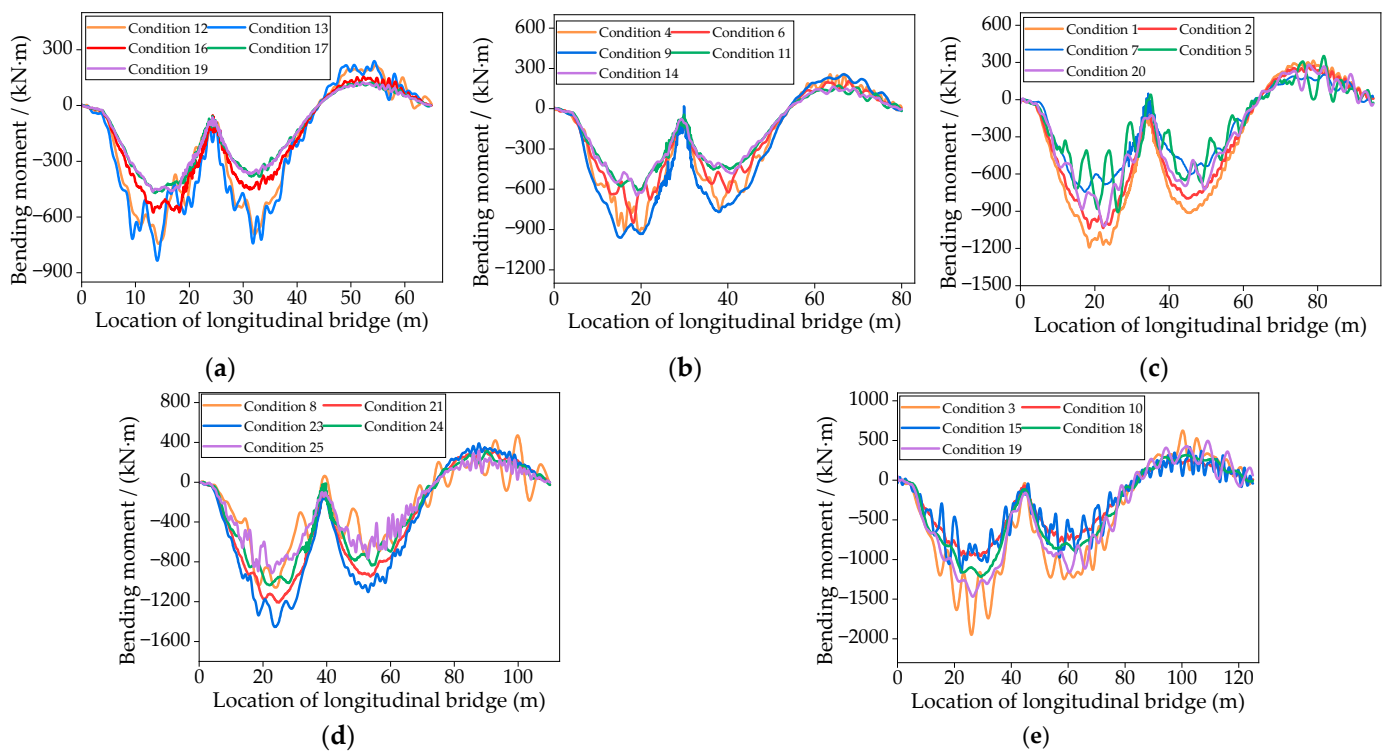
Figure 12. Time-history curves of the negative bending moment in the three-span continuous girder bridges. (**a**) Time-history curves of the bridges with a span of 20 m; (**b**) Time-history curves of the bridges with a span of 25 m; (**c**) Time-history curves of the bridges with a span of 30 m; (**d**) Time-history curves of the bridges with a span of 35 m; (**e**) Time-history curves of the bridges with a span of 40 m.

4. Optimization of the Intercepted Segment for the Weighted DLA

4.1. Intercepted Segments of the Time-History Curve

Take the negative moment time-history curve of Section B as an example; different lengths of the curve were intercepted according to the span length *L* (for example, from the peak of the negative moment of each span, increase the intercept intercepted length in steps of 1/16 *L*). The way of segment interception is shown in Figure 13, and the parameters are shown in Table 3; wherein segment 0 indicates the DLA calculated by the theoretical method.
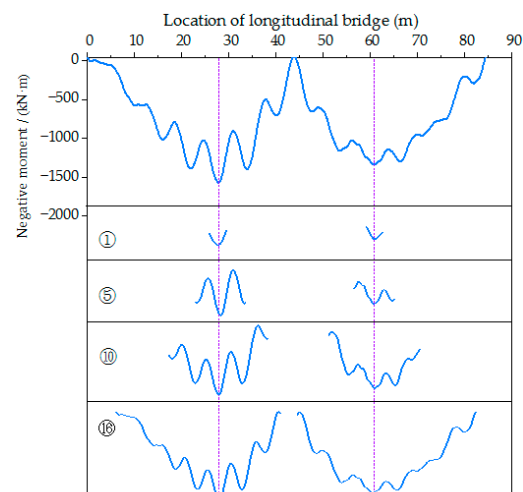

Figure 13. Intercepted segments of time-history curves.

Table 3. Parameters of the segments.

Intercepted Segment Number	Interval Length
0	theoretical method
1	$L/16$
2	$2L/16$
3	$3L/16$
4	$L/4$
5	$5L/16$
6	$3L/8$
7	$7L/16$
8	$L/2$
9	$9L/16$
10	$5L/8$
11	$11L/16$
12	$3L/4$
13	$13L/16$
14	$7L/8$
15	$15L/16$
16	L

Note: No. 1 in the table corresponds to the intercepted segment ①, as shown in Figure 13 and the other segments in turn.

4.2. DLAs by the Weighted Average Method

Each time-history curve was intercepted sequentially according to segment length in Table 3, and the weighted DLAs corresponding to different intercepted segments were obtained from Equation (4), as shown in Figure 14.
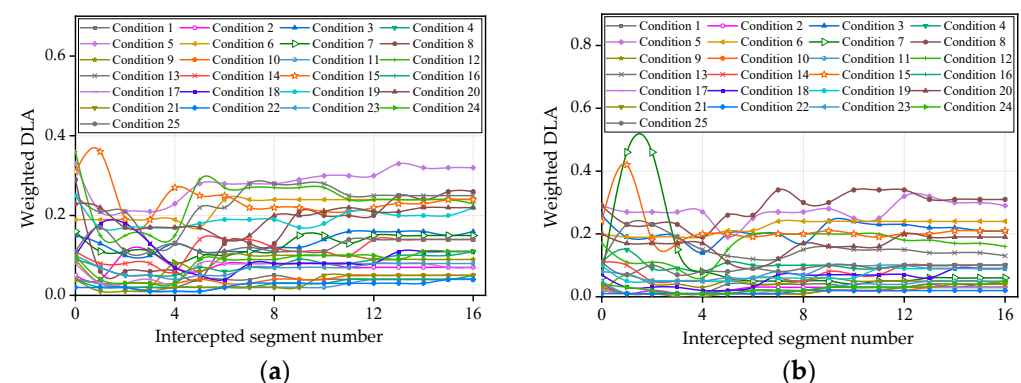

Figure 14. Weighted DLAs of each condition. (**a**) Weighted DLAs for the two-span continuous girder bridge; (**b**) Weighted DLAs for the three-span continuous girder bridges.

In Figure 14, the weighted DLAs fluctuate greatly in the early stage and stabilize in the latter as the segment length increases. The maximum difference of DLA for the same time-history curve between segments 1 and 8 is 0.17, and the maximum difference between segments 9 and 16 is relatively stable, with a maximum difference of 0.06. Overall, The weighted DLAs for the last eight segments are less different than the first eight segments. However, too much data increases the amount of computation, so the segments need to be optimized.

4.3. Differences between Weighted Average Method and Theoretical Method

In the field load test, outliers may occur in the measured data, and the uncertainty and contingency factors interfere with the DLA. However, the time-history curve obtained by numerical simulation doesn't have these problems.

To quantify the difference between the weighted DLA and the theoretical DLA, the second-order central moments describing the characteristics of the data variables were introduced. The weighted DLA could be analogized to the standard value in mathematical

statistics. The weighted DLA of the different intercepted segments under the same time-history curve could be considered a set of samples. The second-order central moment of the weighted DLA D_i^2 is expressed by Equations (15) and (16). The standard deviation of the weighted DLA D_i, which was a square root of D_i^2, as shown in Equation (17), was used to evaluate the dispersion of the weighted DLA from the theoretical DLA in different intercepted segments.

$$\overline{\mu}_i = \sum_{j=1}^{n} \frac{\mu_{ij} Y_{meanij}}{\sum\limits_{j=1}^{n} Y_{meanij}} \quad (i = 1, \ldots, 16 \quad j = 1, \ldots, n) \tag{15}$$

$$D_i^2 = (\overline{\mu}_i - \overline{\mu}_0)^2 \quad (i = 1, \ldots, 16) \tag{16}$$

$$D_i = \sqrt{D_i^2} \tag{17}$$

where $\overline{\mu}_i$ represents the DLA calculated by WAM using the ith intercepted segment; μ_{ij} is the DLA calculated by the experimental method using the jth local band of the ith intercepted segment; n represents the total number of interception segments of a time-history curve; D_i^2 is the second-order central moment of the weighted DLA related to the ith intercepted segment under the same time-history curve; D_i is the standard deviation corresponding to the second-order central moment D_i^2.

The statistics D_i for each condition in Table 2 were performed to make the variation of the standard deviation of weighted DLA $\overline{\mu}$ more representative. Linear normalization was used to eliminate the influence caused by dimensional differences. The overall trend in the difference between weighted DLA and theoretical DLA was characterized using the total effect of the standard deviation, which was denoted as offset moment K. The specific operation processes are as follows:

(1) First, the standard deviations of each time-history curve D_i are compiled into an array and normalized;
(2) Then, the normalized standard deviations D_i^{norm} with the same number in different time-history curves are added to obtain the offset moment K_i (Equation (18)), and the calculation results are shown in Figure 15.
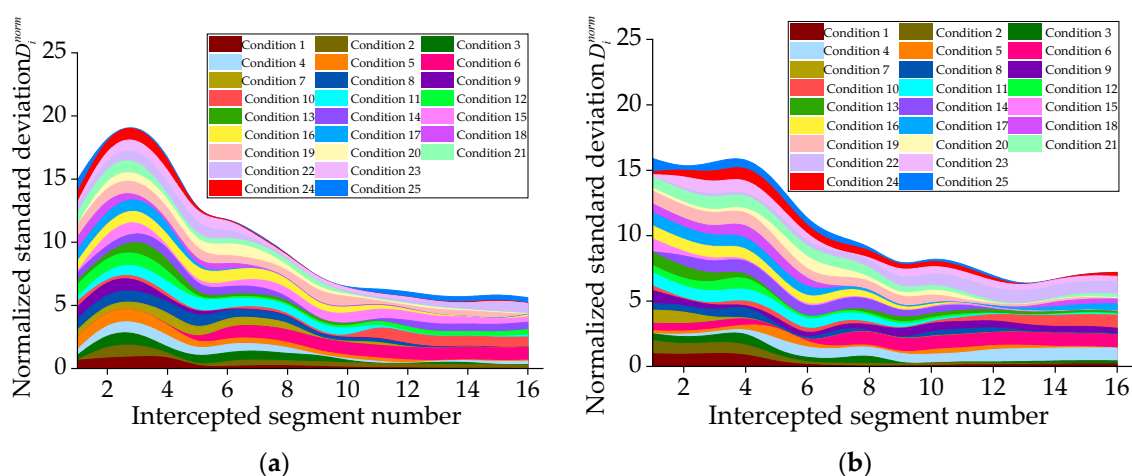
$$K_i = \sum_{m=1}^{9} D_m^2 \tag{18}$$

Figure 15. Normalized standard deviation D_i^{norm} and offset moment K of the weighted DLAs. (**a**) Results for two-span continuous gird bridge; (**b**) Results for three-span continuous gird bridge.

The offset moment K reflects the standard deviation D_i^{norm} in all conditions. The smaller the standard deviation D_i^{norm}, the smaller the difference between the weighted DLA and the theoretical DLA. In Figure 15, the 2nd to 4th intercepted segments have the largest offset moment K of 19.50, which indicates that the weighted DLA deviates significantly from the theoretical DLA. The offset moment K of the 10th to 16th intercepted segments is between 5.61 and 8.45, which are smaller than other intercepted segments. From the above, the weighted DLAs calculated using the intercepted segment lengths of $10L/16$ to L are closer to the theoretical DLAs.

4.4. Variability of DLAs by the Weighted Average Method

A coefficient of variation was introduced to study the relationship between the variability of weighted DLA and the segment length. The variation coefficients of each intercepted segment v_i were obtained according to all local bands to evaluate the stability of weighted DLAs. The specific operation processes are as follows:

(1) First, the weighted DLAs of each intercepted segment in Figure 14 are substituted to Equation (19), and the weighted variance σ_i^2 after considering the magnitude of each segment is obtained. Next, the weighted standard deviation σ_i is obtained by opening the square of the weighted variance σ_i^2;

(2) The coefficients of variation v_i for different segments were obtained by substituting the weighted standard deviations σ_i into Equation (21), and the results are shown in Figure 16.

$$\sigma_i^2 = \sum_{j=1}^{n} \frac{\left(\mu_{ij} - \overline{\mu_{ij}}\right)^2 Y_{meanij}}{\sum\limits_{j=1}^{n} Y_{meanij}} \quad (i = 1, \ldots, 16 \quad j = 1, \ldots, n) \tag{19}$$

$$\sigma_i = \sqrt{\sigma_i^2} \tag{20}$$

$$v_i = \frac{\sigma_i}{\overline{\mu_i}} \tag{21}$$

where σ_i^2 is the variance of the weighted DLA for the ith intercepted segment, which is simply referred to as weighted variance; σ_i is the standard deviation of the weighted DLA for the ith intercepted segment, which is denoted to as weighted standard deviation; v_i is the coefficient of variation of the weighted DLA for the ith intercepted segment.
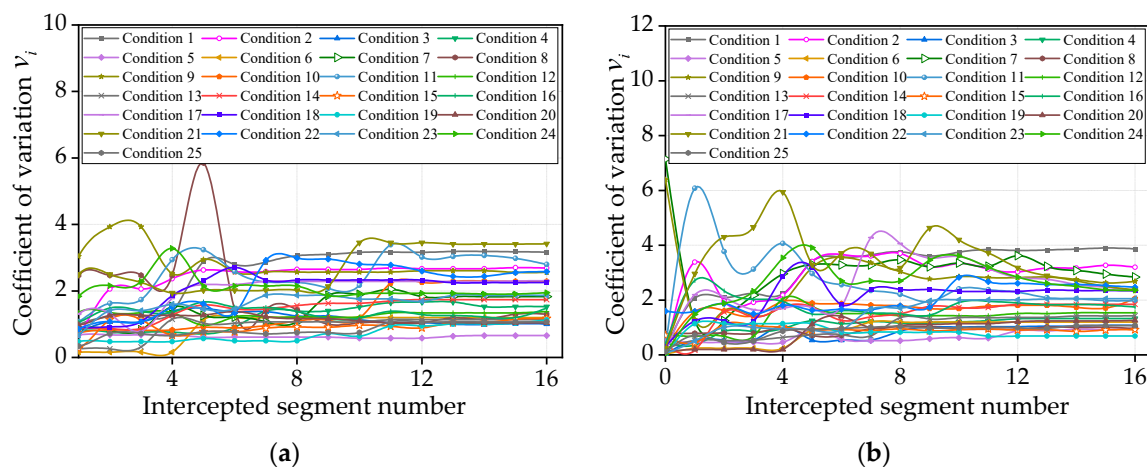

Figure 16. Coefficients of variation of the weighted DLA. (**a**) Coefficients of variation for two-span continuous gird bridge; (**b**) Coefficients of variation for three-span continuous gird bridge.

In Figure 16, the variation coefficients of the intercepted segments for most conditions fluctuate greatly at the beginning. Among them, the maximum value is 6.08. Then the

coefficients of variation gradually stabilize as the weighted segment length increases. The maximum difference in the coefficient of variation between the 1st and 9th segments of the same condition for the two-span continuous girder bridge is 5.85, while the maximum difference in coefficients of variation between the 10th and 16th segments is 1.22. The maximum difference in the coefficient of variation between the 1st and 9th segments of the same condition for the three-span continuous girder bridge is 5.89, while the maximum difference in coefficients of variation between the 10th and 16th segments is 1.82. The trends for two-span continuous girder bridges and three-span continuous girder bridges are almost identical. The results show that the weighted DLA calculated using the 1st to the 9th segment is not stable enough. The segment with a relatively small value and stable coefficient of variation should be selected if possible.

In summary, the optimal intercepted segment of the weighted DLA for the negative bending moment is to consider the effect of the dispersion of weighted DLA and the stability of the WAM for a comprehensive comparison. Under the same segment number, the offset moments of the 10th and 16th segments for the 25 conditions are relatively small, and the value is closer to the theoretical DLA. Meanwhile, the coefficients of variation of these segments are more stable than in the first nine segments. Therefore, the intercepted segment length of $9L/16$ to L is suitable as the optimal segment for calculating the weighted DLA of the negative moment in a continuous girder bridge. Moreover, it is recommended to use the re-averaging of the DLAs of these seven segments.

4.5. Ability to Resist Outliers

As shown in [12], a small amount of outliers frequently occurs in measured signals during field tests, and the corresponding data set was referred to as "bad data". The WAM had the advantage of minimizing the effect of outliers on DLA. To evaluate the ability of the WAM to resist "bad data," the outliers were created by artificially adjusting the amplitude of a small number of points. Taking the time-history curves of condition 3 in two types of continuous gird bridges as examples, two factors were considered in creating "bad data" one was the ratio α of outliers (ratio of the number of outliers in the whole data set). The other was the multiple k of the outlier amplitude (a multiple of the amplitude of the outliers to their raw amplitude after adjustment). Considering the ratio α of outliers as 5%, 10%, 15%, 20%, 15%, and the multiple k of the outlier amplitude as 1.1 times, 1.2 times, 1.3 times, 1.4 times, 1.5 times, the DLAs with different "bad data" are shown in Figure 17.
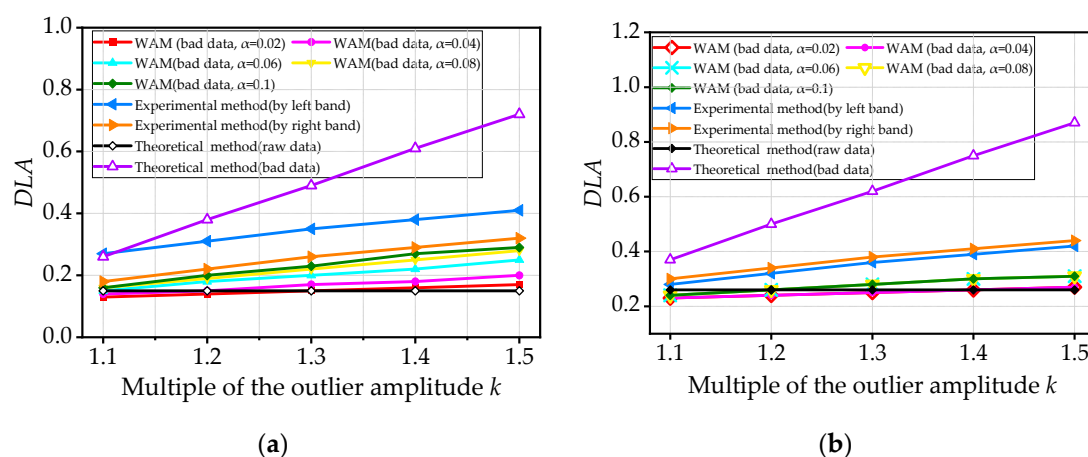

Figure 17. Comparison of DLA with different data. (**a**) DLAs for two-span continuous girder bridge; (**b**) DLAs for three-span continuous girder bridge.

In Figure 17, the truth DLA was obtained from the raw data using the theoretical method, while the weighted DLA was obtained by averaging the weighted DLAs of the segments $10L/16$ to L. The maximum error between the DLAs calculated by Equation (2) and the truth DLA in the two types of continuous gird bridge is 381.3% when the multiple

k of outlier amplitude is 1.5 times. At the same time, the maximum error between the weighted DLA and the truth DLA is only 96.4%. The maximum error between the DLA calculated by Equation (3) and the truth DLA of the two bridges is 75.2% when the multiple of outlier amplitude k is 1.1 times. At the same time, the maximum error between weighted DLA and true DLA is only 12.0%. The error between the weighted DLA and the truth DLA increases with the outlier ratio α and outlier amplitude multiple k. As the outlier ratio α and outlier amplitude multiple k change, the experimental method has an error of 8.3% to 172.8% with the truth DLA, while the error of the weighted DLA range from 0.1% to 96.4%. The error between the weighted DLA and the true DLA is always smaller than the experimental method under the same conditions. The above results show that the WAM has strong "outlier filtering" ability in the " bad data" processing.

5. Strategies for Accurately Assessing Bridge DLA

5.1. Measurement

The choice of sensor is critical to acquiring the DLA based on the measurement target (dynamic response). Deflection and strain are the most common measurement targets for a bridge's dynamic response [33,35]. For deflection, a distinction needs to be made between stiff bridges (main natural frequency f < 1 Hz, deflection at millimeter or sub-millimeter level) and flexible bridges (main natural frequency f > 1 Hz, deflection at centimeter or decimeter level) [12]. Normally, devices or methods such as dial gauge and LDTV have high SNR (signal-to-noise ratio) and reliable results in stiff bridge's dynamic deflection measurement [36–38]. Meanwhile, geodetic techniques (GPS/GNSS) [39,40], microwave radar interferometry [41,42], terrestrial laser scanning (TLS) [43], and vision-based optical methods [44] perform well in flexible or large span bridges due to high SNR in a large deflection.

For strain measurement, it is necessary to differentiate between steel and concrete bridges according to the structural material. For steel bridges, the strain value is usually larger, and fiber-optic strain gauges, resistive strain gauges, and double-cantilever strain gauges can be used. Meanwhile, for concrete bridges, fiber-optic strain gauges and dual-cantilever strain gauges are appropriate to measure the bridge's dynamic strain to obtain signals with high SNR [45]. Resistance strain gauges have high sensitivity and are highly influenced by temperature and humidity in the field environment.

The sampling frequency is also an important factor affecting the measurement results. According to the Nyquist–Shannon sampling theorem, the sampling rate has to be at least twice as high as the fundamental frequency to estimate the frequency [3,46,47]. In the sampling with strict requirements on the peak value, it is still necessary to increase the sampling rate further. The signal peak value obtained by 8 to 10 times the sampling rate is close to the real signal (Figure 18), which can avoid signal aliasing while capturing the full dynamic response of the structure [35,48].
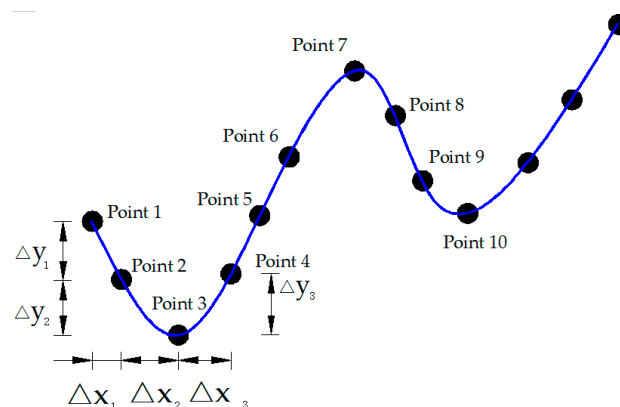

Figure 18. Discrete signal.

In addition, the dynamic response of the bridge without external load excitation should be collected during the measurement, and the SNR of the measured signal could be initially estimated by the signal-to-noise indicator ε, as shown in Equation (22) and Figure 19. Empirically, a more accurate DLA could be obtained when $\varepsilon < 0.02$. After the above conditions are met, dynamic response measurement could be carried out.

$$\varepsilon = \frac{\Delta Y}{2Y_{st}} \tag{22}$$

where ε is signal-to-noise indicator; ΔY represents the range of initial signal amplitude; Y_{st} is the amplitude of the measured static response.
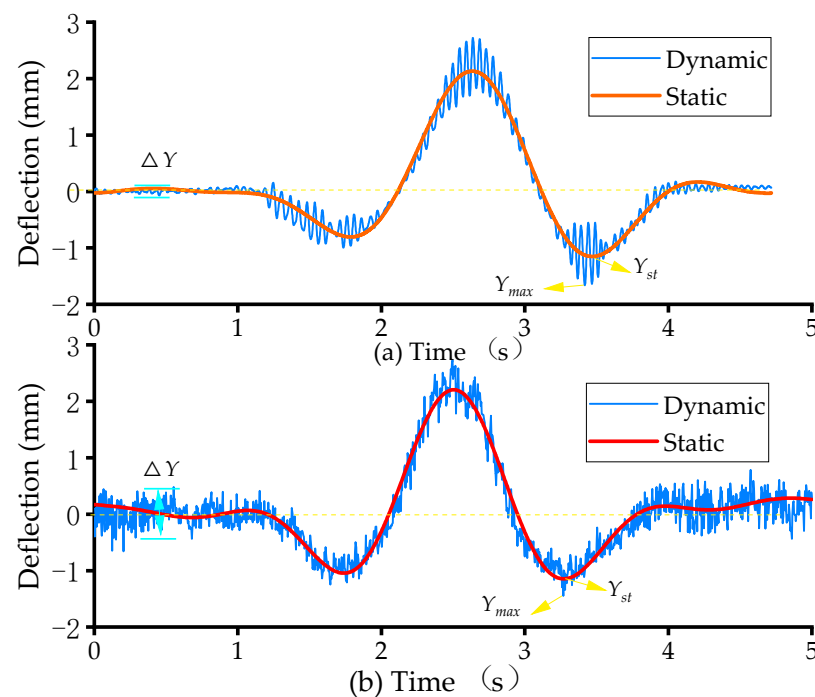

Figure 19. Deflections measured by different methods.

5.2. Data Processing

After obtaining the data, it should be set as the filtering cut-off frequency based on the vibration participation mass ratio first to filter out the white noise and the higher order mode signals with a lower contribution. Usually, the modes with 95% of the participating mass can be selected as the cut-off frequency. A time-continuous derivative of the signal is performed to obtain the velocity and velocity response. If a very obvious peak point appears, it indicates that the signal at the point extremely near the point is an outlier and should be excluded. The theoretical method to calculate the DLA is the best choice when the signal is good. The WAM is recommended to calculate the DLA when the signal has outliers at the peak point, and either exclusion or retention greatly influences the results.

6. A Case of DLA Measurement

A 3 × 30 m precast box-girder bridge on the Anlan Highway (Shaanxi Province, China) was carried out as a case of DLA measurement to verify the applicability of the WAM. The cross-section of the bridge is shown in Figure 20. Strain gauges were pasted at the bottom plate of the girder in the negative moment zone of the fulcrum section. One unilateral wheel of a 36-ton vehicle slowly crossed the bridge along the white boundary of the travel lane to obtain the maximum static strain. Then, a vehicle excitation was carried out, and the lateral driving position was strictly controlled in the same way as the above static test.

The sampling frequency was 200 Hz, and the measurement details are shown in Figure 21. The dynamic tests were carried out three times for representativeness.
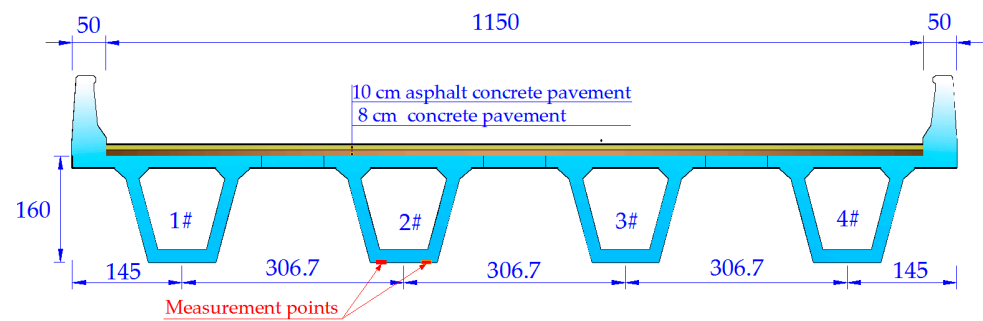

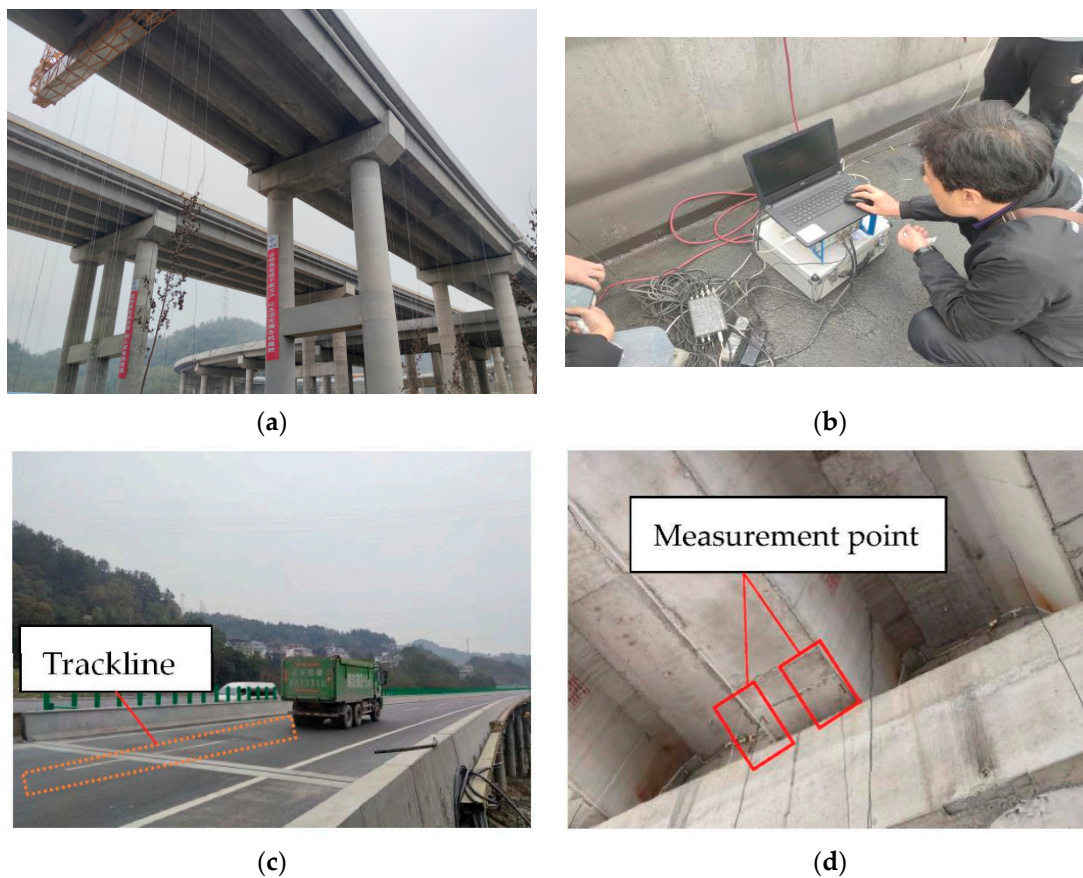**Figure 20.** Cross-section dimensions of the bridge (unit: cm).

Figure 21. Representative photographs of the static and dynamic load tests. (**a**) Bridge appearance; (**b**) Data acquisition process; (**c**) Static and dynamic load tests; (**d**) Strain sensor arrangement.

The measurement data were checked according to Section 5.2. After determining that there were no outliers, DLAs were calculated using the theoretical, the WAM, the experimental, and the low-pass filtering methods. The results are shown in Figure 22. Among them, the spectrum was obtained by FFT (fast Fourier transform) of dynamic strain for filtering (Figure 23). Then, the right side of the first main lobe in the power spectrum was regarded as the cut-off frequency, and the quasi-static strains were obtained by filtering at 1, 1.6, and 1 Hz in three measurements, respectively [49].
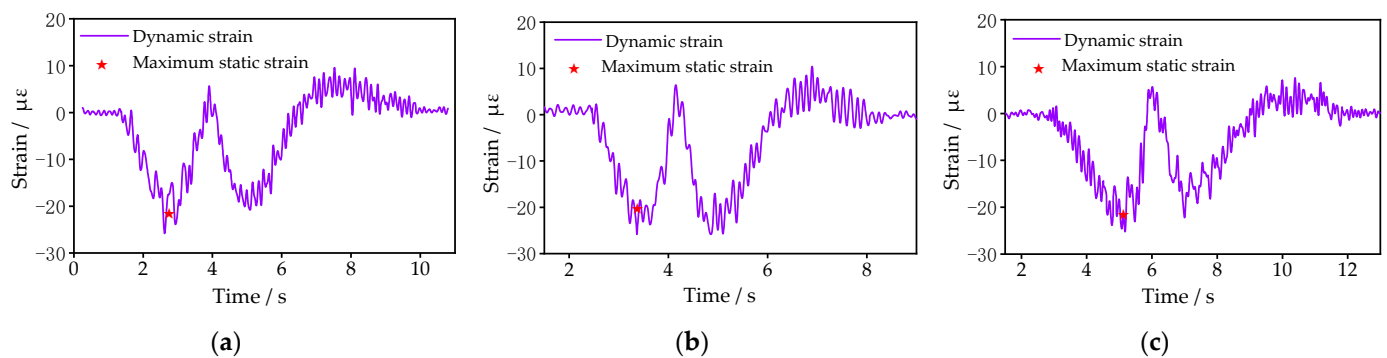
Figure 22. Measured dynamic strain of the bridge. (**a**) Response of the negative bending moment strain for the first measurement; (**b**) Response of the negative bending moment strain for the second measurement; (**c**) Response of the negative bending moment strain for the third measurement.
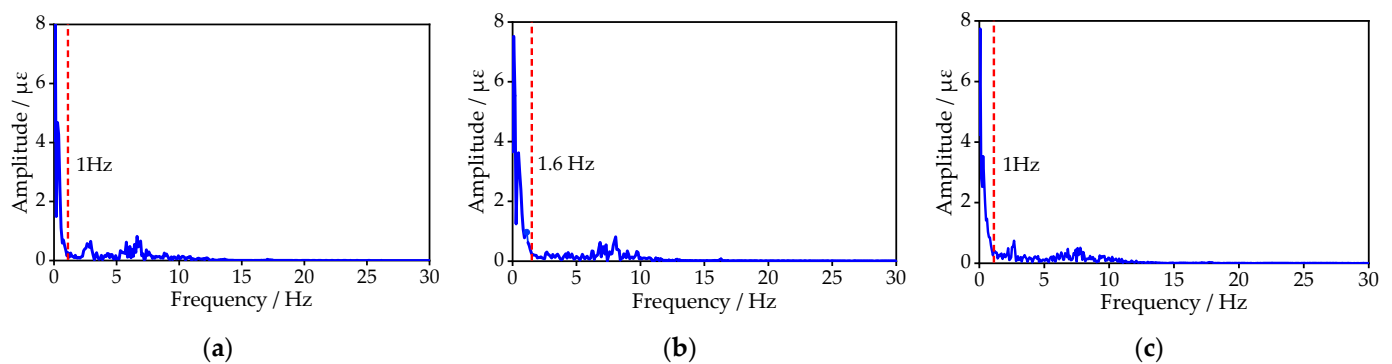

Figure 23. Power spectrum of the measured strain response. (**a**) Power spectrum for the first measurement; (**b**) Power spectrum for the second measurement; (**c**) Power spectrum for the third measurement.

In Figure 24, the average error in the three measurements between the weighted DLAs and the theoretical DLAs is 6.5%, and the maximum error is 12.9%. The errors between the experimental and theoretical methods in DLAs range from 4.2% to 73.9%, with a large dispersion due to a left or right band selection. The errors between the low-pass filtering and the theoretical method in DLAs range from 4.5% to 65.2%. Nonetheless, the error of the DLA calculated by WAM is smaller than that of the experimental and filtering methods.
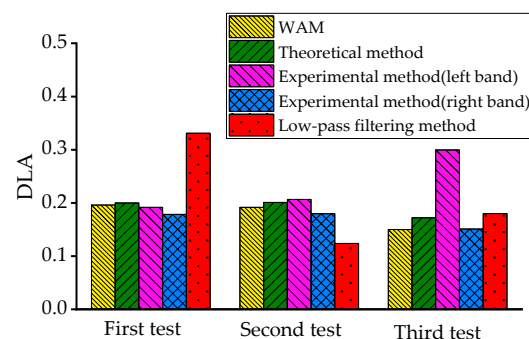

Figure 24. Comparison of DLAs from various methods.

A combination of dynamic and static load tests is the most reliable method under strictly controlled conditions. However, it is not easily adopted by engineers in practice due to time and cost. The WAM is difficult to obtain extreme values because of the multi-point effect, which usually floats around the theoretical value. When the combination of dynamic and static tests is not achieved, such as random traffic, the weighted DLA has

higher measurement accuracy than the experimental and low-pass filtering methods. The WAM, which can fully account for the impact effects of multiple locations (even multiple moving loads) instead of single-point, could eliminate the accidental error introduced by external factors or randomness of road surface conditions. The research of the WAM in continuous girder bridges with negative bending moments will further expand the scope of the WAM applications.

Moreover, further improve the efficiency of dynamic and static load test, such as the employment of wireless data acquisition and non-contact measurement, which helps to adopt the theoretical method. The low-pass filtering method still needs to be combined with experiments to further research the "dynamic-static" response separation technique that can improve the accuracy and reliability of extracting the static response. The experimental method is recommended for use in many repeated dynamic load tests rather than in a single test. The average result of multiple tests under the same conditions should be taken as the DLA. Combining the WAM method and signal noise-reduction technique would further improve the accuracy of weighted DLA.

7. Conclusions

The intercepted segments of the negative moment response for the weighted DLAs were optimized for the first time based on the offset moment and variation coefficient in the precast continuous box-girder bridge. The ability of the WAM to resist outliers was evaluated. Finally, the applicability of WAM to calculate DLAs was verified by a measurement case. The conclusions were drawn as follows:

(1) In the negative bending moment of precast concrete continuous girder bridges, the offset moment first increased and then decreased. At the same time, the weighted DLAs and the variation coefficient fluctuated greatly in the early stage and stabilized in the latter as the weighted segment length increased. The intercepted segments of 10/16 to 1 times the span length were suitable for the WAM to calculate the negative bending moment DLA due to small offset moments and stable variation coefficients. Moreover, it is recommended to use the re-averaging of the DLAs of these seven segments. When artificially creating outliers for valid data, the error between the weighted DLA and the truth DLA increased with the outlier ratio and outlier amplitude multiple. Thus, the WAM has a strong anti-interference ability against outliers in "bad data".

(2) In field tests, the choice of sensor is critical to acquiring the DLA based on the measurement target. Thus, it is necessary to distinguish between stiff and flexible bridges for deflection measurement and between steel and concrete structures for strain measurement. The minimum sampling frequency of 8~10 times concerned high-order frequency of a structure should be satisfied to obtain accurate DLAs. The ratio of the initial signal amplitude range to the estimated static response could be used as a basis for a quick assessment of the SNR. After obtaining the measurement data, the modes with 95% of the participating mass can be selected as the cut-off frequency to filter out white noise and higher-order modes with a lower contribution. Then, the collected signal was used to derive the time sequentially to obtain the velocity and velocity response and identify outliers.

(3) The DLAs obtained by the WAM have less dispersion than the experimental and low-pass filtering methods. In three measurements of a field bridge, the error ranges of the DLAs obtained by the WAM, the experimental method, and the low-pass filter method from the theoretical DLAs were 1.1% to 26.5%, 7.6% to 98.6%, and 7.3% to 85.5%, respectively. When the combination of dynamic and static tests is not achieved, the weighted DLA has higher measurement accuracy than the experimental and low-pass filtering methods. The WAM can fully account for the impact effects of multiple locations (even multiple moving loads) instead of single-point, which could eliminate the accidental error introduced by external factors or randomness of road

surface conditions. Moreover, combining the WAM method and signal noise-reduction technique would further improve the accuracy of weighted DLA.

(4) The theoretical method was recommended in numerical simulation; however, the data may be affected by the external environment or power frequency in a field. There was great randomness and uncertainty in using it to calculate a DLA. The different choices of the left and right bands could lead to significant differences in the DLAs calculated by the experimental method, which is recommended for use in many repeated dynamic load tests. When the period of static oscillations matches the period of dynamic oscillations, the filtering method to calculate DLA will fail. The weighted DLA can fully consider the overall impact effect of the vehicle on a bridge, which was closer to the existing structural design concept; meanwhile, it has a great advantage in eliminating the interference of external factors.

It should, however, be noted that the WAM does not always obtain the most unfavorable effect of DLAs, but will minimize the measurement error between the two after optimization and ensure that extreme value does not occur. The research of the WAM in continuous girder bridges with negative bending moments will further expand the scope of the WAM applications.

Author Contributions: Conceptualization, J.T.; Data curation, Y.W. and Y.Z. (Yongjun Zhou); Formal analysis, Y.W. and K.M.; Funding acquisition, Y.W. and Y.Z. (Yongjun Zhou); Investigation, Y.W. and Y.Z. (Yongjun Zhou); Methodology, Y.W.; Project administration, J.T.; Resources, J.T. and K.M.; Software, Y.W.; Supervision, Y.Z. (Yongjun Zhou) and Y.Z. (Yu Zhao); Validation, Y.Z. (Yongjun Zhou); Visualization, Y.Z. (Yu Zhao); Writing—original draft, Y.W.; Writing—review & editing, J.T., Y.Z. (Yongjun Zhou), Y.Z. (Yu Zhao), W.F. and K.M. All authors have read and agreed to the published version of the manuscript.

Institutional Review Board Statement: Not applicable.

Informed Consent Statement: Not applicable.

Data Availability Statement: Data is contained within the article.

Conflicts of Interest: The authors declare no conflict of interest.

References

1. Mclean, D.I.; Marsh, M.L. *Dynamic Impact Factors for Bridges*; Transportation Research Board National Research Council, Ltd.: Washington, DC, USA, 1998; Volume 266.
2. Clarke, S.N.; Deatherage, J.H.; Goodpasture, D.W.; Burdette, E.G. Influence of bridge approach, surface condition, and velocity on impact factors for fatigue-prone details. *Transp. Res. Rec.* **1998**, *1624*, 166–179. [CrossRef]
3. Paultre, P.; Chaallal, O.; Proulx, J. Bridge dynamics and dynamic amplification factors—A review of analytical and experimental findings. *Can. J. Civ. Eng.* **1992**, *19*, 260–278. [CrossRef]
4. Jung, H.; Kim, G.; Park, C. Impact factors of bridges based on natural frequency for various superstructure types. *KSCE J. Civ. Eng.* **2013**, *17*, 458–464. [CrossRef]
5. Deng, L.; Yu, Y.; Zou, Q.L.; Cai, C.S. State-of-the-art review of dynamic impact factors of highway bridges. *J. Bridge Eng.* **2014**, *20*, 04014080. [CrossRef]
6. *JTG D60-2015*; General Code for Design of Highway Bridges and Culverts. Ministry of Transport of the People's Republic of China (MTPRC): Beijing, China, 2015.
7. *JRA(1996)*; Specifications for Highway Bridges. Part 1: Common Specifications. Japan Road Association: Tokyo, Japan, 2012.
8. *AASHTO(2017)*; LRFD Bridge Design Specifications. American Association of State Highway and Transportation Officials Specifications: Washington, DC, USA, 2017.
9. Bakht, B.; Pinjarkar, S.G. Review of dynamic testing of highway bridges—A review. *Transp. Res. Rec.* **1989**, *1223*, 93–100.
10. Kim, Y.J.; Tanovic, R.; Wight, R.G. Recent advances in performance evaluation and flexural response of existing bridges. *J. Perform. Constr. Facil.* **2009**, *23*, 190–200. [CrossRef]

11. Zhou, Y.J.; Ma, Z.J.; Zhao, Y.; Shi, X.W.; He, S.H. Improved definition of dynamic load allowance factor for highway bridges. *Struct. Eng. Mech.* **2015**, *54*, 561–577. [CrossRef]
12. Stiros, S.C. GNSS (GPS) Monitoring of dynamic deflections of bridges: Structural constraints and metrological limitations. *Infrastructures* **2021**, *6*, 23. [CrossRef]
13. GangaRao, H.V.S. Impact factors for highway bridges. In *Vehicle, Tire, Pavement Interface*; ASTM International: Pennsylvania, PA, USA, 1992; Volume 1164.
14. Kwasniewski, L.; Wekezer, J.; Roufa, G.; Li, H.; Ducher, J.; Malachowski, J. Experimental evaluation of dynamic effects for a selected highway bridge. *J. Perform. Constr. Facil.* **2006**, *20*, 253–260. [CrossRef]
15. Rezaiguiam, A.; Ouelaa, N.; Laefer, D.F.; Guenfoud, S. Dynamic amplification of a multispan, continuous orthotropic bridge deck under vehicular movement. *Eng. Struct.* **2015**, *100*, 718–730. [CrossRef]
16. Liu, B.; Wang, Y.Z.; Hu, P.; Yuan, Q. Impact coefficient and reliability of mid-span continuous beam bridge under action of extra heavy vehicle with low speed. *J. Cent. South Univ.* **2015**, *22*, 1510–1520. [CrossRef]
17. Ma, F.; Feng, D.; Zhang, L.; Yu, H.; Wu, G. Numerical investigation of the vibration performance of elastically supported bridges under a moving vehicle load based on impact factor. *Int. J. Civ. Eng.* **2022**, 1–16. [CrossRef]
18. Gao, Q.F.; Wang, Z.L.; Li, J.; Chen, C.; Jia, H.Y. Dynamic load allowance in different positions of the multi-span girder bridge with variable cross-section. *J. Vibro. Eng.* **2015**, *17*, 2025–2039.
19. Deng, L.; He, W.; Shao, Y. Dynamic impact factors for shear and bending moment of simply supported and continuous concrete girder bridges. *J. Bridge Eng.* **2015**, *20*, 04015005. [CrossRef]
20. Li, H.; Wekezer, J.; Kwasniewski, L. Dynamic response of a highway bridge subjected to moving vehicles. *J. Bridge Eng.* **2008**, *13*, 439–448. [CrossRef]
21. Azimi, H.; Galal, K.; Pekau, O.A. A modified numerical VBI element for vehicles with constant velocity including road irregularities. *Eng. Struct.* **2011**, *33*, 2212–2220. [CrossRef]
22. Beben, D. Dynamic amplification factors of corrugated steel plate culverts. *Eng. Struct.* **2013**, *46*, 193–204. [CrossRef]
23. Johnson, D.E.; Johnson, J.R.; Moore, H.P. *A Handbook of Active Filters*; PrenticeHall: Englewood Cliffs, NJ, USA, 1980; pp. 193–201.
24. Calcada, R.; Cunha, A.; Delgado, R. Analysis of traffic-in-duced vibrations in a cable-stayed bridge. Part i: Experi-mental assessment. *J. Bridge Eng.* **2005**, *10*, 370–385. [CrossRef]
25. Ashebo, D.B.; Chan, T.; Yu, L. Evaluation of dynamic loads on a skew box girder continuous bridge part i: Field testand modal analysis. *Eng. Struct.* **2007**, *29*, 1052–1063. [CrossRef]
26. Lu, Y.J. Research on Dynamics of Heavy Vehicle and Road Surface Interaction. Ph.D. Thesis, Beijing Jiaotong University, Beijing, China, 2010.
27. Deng, L.; Duan, L.L.; He, W.; Ji, W. Study on vehicle model for vehicle-bridge coupling vibration of highway bridges in China. *China J. Highw. Transp.* **2018**, *31*, 92–100.
28. Turkyilmazoglu, M. An optimal analytic approximate solution for the limit cycle of Duffing–van der Pol equation. *J. Appl. Mech.* **2011**, *78*, 856–875. [CrossRef]
29. Turkyilmazoglu, M. The Airy equation and its alternative analytic solution. *Phys. Scr.* **2012**, *86*, 055004. [CrossRef]
30. Aljahdaly, N.H.; Akgül, A.; Shah, R.; Mahariq, I.; Kafle, J. A comparative analysis of the fractional-order coupled Korteweg-De Vries equations with the Mittag-Leffler law. *J. Math.* **2022**, *2022*, 8876149. [CrossRef]
31. Nonlaopon, K.; Naeem, M.; Zidan, A.M.; Shah, R.; Gumaei, A. Numerical investigation of the time-fractional Whitham-Broer-Kaup equation involving without singular kernel operators. *Complexity* **2021**, *2021*, 7979365. [CrossRef]
32. Areshi, M.; Khan, A.; Shah, R.; Nonlaopon, K. Analytical investigation of fractional-order Newell-Whitehead-Segel equations via a novel transform. *AIMS Math.* **2022**, *7*, 6936–6958. [CrossRef]
33. Ma, L.; Zhang, W.; Han, W.S.; Liu, J.X. Determining the dynamic amplification factor of multi-span continuous box girder bridges in highways using vehicle-bridge interaction analyses. *Eng. Struct.* **2019**, *181*, 47–59. [CrossRef]
34. Chen, X.D. The Vehicle-Bridge Interaction Analysis of Corrugated Steel Web Box Girder Based on Contact-Constraint Method. Master's Thesis, Chongqing University, Chongqing, China, 2019.
35. Schwarz, M.; Laman, J.A. Response of prestressed concrete i-girder bridges to live load. *J. Bridge Eng.* **2001**, *6*, 1–8. [CrossRef]
36. Nassif, H.H.; Gindy, M.; Davis, J. Comparison of laser doppler vibrometer with contact sensors for monitoring bridge deflection and vibration. *NDT E Int.* **2005**, *38*, 213–218. [CrossRef]
37. Moreu, F.; Jo, H.; Li, J.; Kim, R.E.; Cho, S.; Kimmle, A.; LaFave, J.M. Dynamic assessment of timber railroad bridges using displacements. *J. Bridge Eng.* **2015**, *20*, 04014114. [CrossRef]
38. Hannan, M.A.; Hassan, K.; Jern, K.P. A review on sensors and systems in structural health monitoring: Current issues and challenges. *Smart Struct. Syst.* **2018**, *22*, 509–525.
39. Xi, R.; He, Q.; Meng, X. Bridge monitoring using multi-GNSS observations with high cutoff elevations: A case study. *Measurement* **2021**, *168*, 108303. [CrossRef]
40. Yu, J.; Meng, X.; Yan, B.; Xu, B.; Fan, Q.; Xie, Y. Global navigation satellite system-based positioning technology for structural health monitoring: A review. *Struct. Control Health Monit.* **2020**, *27*, e2467. [CrossRef]
41. Pedrini, G.; Osten, W.; Gusev, M.E. High-speed digital holographic interferometry for vibration measurement. *Appl. Opt.* **2006**, *45*, 3456–3462. [CrossRef]

42. Pieraccini, M.; Parrini, F.; Fratini, M.; Atzeni, C.; Spinelli, P.; Micheloni, M. Static and dynamic testing of bridges through microwave interferometry. *NDT E Int.* **2007**, *40*, 208–214. [CrossRef]

43. Artese, S.; Zinno, R. TLS for dynamic measurement of the elastic line of bridges. *Appl. Sci.* **2020**, *10*, 1182. [CrossRef]

44. Park, J.W.; Moon, D.S.; Yoon, H.; Gomez, F.; Spencer, B.F., Jr.; Kim, J.R. Visual-inertial displacement sensing using data fusion of vision-based displacement with acceleration. *Struct. Control. Health Monit.* **2018**, *25*, e2122. [CrossRef]

45. Scott, R.H.; Banerji, P.; Chikermane, S.; Srinivasan, S.; Basheer, P.M.; Surre, F.; Grattan, K.T. Commissioning and evaluation of a fiber-optic sensor system for bridge monitoring. *IEEE Sens. J.* **2013**, *13*, 2555–2562. [CrossRef]

46. Butzer, P.L.; Stens, R.L. Sampling theory for not necessarily band-limited functions: A historical overview. *SIAM Rev.* **1992**, *34*, 40–53. [CrossRef]

47. Kist, A.M.; Dürr, S.; Schützenberger, A.; Döllinger, M. OpenHSV: An open platform for laryngeal high-speed videoendoscopy. *Sci. Rep.* **2021**, *11*, 13760. [CrossRef] [PubMed]

48. Higgins, J.R. *Sampling Theory in Fourier and Signal Analysis: Foundations*; Oxford University Press: New York, NY, USA, 1996.

49. Li, W.Z.; Zhang, W.; Wang, Z.L.; Li, Y.; Wang, Y.X. A method for calculation of tested impact of a simply supported girder bridge based on low-pass filtering. *J. Vib. Shock* **2012**, *31*, 46–50.